# 2D-NANOLATTICES

FP7-ICT-2009-C (FET Open)

***Highly anisotropic graphite-like semiconductor/dielectric 2D nanolattices***

## Deliverable D1.3

***Impact of Strain on the Properties of Silicene and Germanene***

**Report prepared by B. van den Broek, E. Scalise, M. Houssa (KU Leuven)**

**Contributors: KU Leuven**

Preparation Date: 27/11/2012

Report version number: final

Classification: Public

Contract Start Date: 01/06/2011

Duration: 36 months

Project Coordinator: NCSR- D (*Dr. A. Dimoulas*)

Contractors: IMEC, KULeuven, CNR, CNRS, U. Marseille

**Project funded by the European Community under the "Future and Emerging Technologies" Programme**

| D1.3 Participant | MM/planned | MM/actual |
|---|---|---|
| KULeuven (lead) | 4 | 4 |

## Table of Content

## 1. Introduction

Ever since its inception in 2004, research into graphene has been ever increasing [1]; now research into other possible 2D materials such as silicene, $MoS_2$, germanene, BN etc. has picked up steam. Silicene and germanene are the silicon and germanium analogues of graphene, respectively. Recently, compelling structural and electronic experimental evidence of the existence of (3x3) silicene superstructure on Ag(111) substrates has been reported [2,3] as well as on a $ZrB_2$ substrate [4].

Following its graphene counterpart, free-standing silicene and germanene both exhibit the characteristic hexagonal lattice with a Si-Si (Ge-Ge) bondlength of 2.30 Å [5] (2.44 Å [6]). Considering the hexagonal lattice, two triangular sublattices can be identified (A and B) both yielding equivalent dispersion near the Brillouin zone symmetry points *K* and *K'* - so-called valley degeneracy. The energy dispersion near these points is linear with zero gap at the Fermi level; the Dirac cone. The calculated Fermi velocity at the Dirac cones is $1.6 \times 10^6$ $ms^{-1}$ for silicene [5] and $1.7 \times 10^6$ $ms^{-1}$ for germanene [6]; it should be pointed out that the dirac cone of silicene was recently observed from ARPES experiments on Ag(111)/silicene interfaces, the extracted Fermi velocity ($1.3 \times 10^6$ $ms^{-1}$) being in excellent agreement with the calculated one.

Considering a nearest-neighbour tight binding model, charge carriers situated at sublattice A only couple to sublattice B, prompting the Dirac Hamiltonian:

$$H = \hbar v_F \left( \sigma_x \delta k_x \pm \sigma_y \delta k_y \right) \tag{1}$$

with $v_F$ the Fermi velocity, $\sigma$ the Pauli matrix and $\delta k$ the wavevector with respect to the *K* and *K'* points; the plus/minus indicates electrons/holes. The sublattice symmetry is manifested by the absence of diagonal elements in equation (1).

In order to exploit the remarkable electronic and mechanical properties of this material, functionalization by introducing a band gap is paramount [7]. By breaking the sublattice symmetry, i.e. valley polarization, a mass term *m* is introduced [8]:

$$H = \hbar v_F \left( \sigma_x \delta k_x \pm \sigma_y \delta k_y \right) + m v_F^2 \sigma_z \tag{2}$$

Contrary to graphene, silicene and germanene are not purely $sp^2$ bonded, but have an out-of-

plane buckling (0.44 Å for silicene; 0.64 Å for germanene [9]) and thus have mixed $sp^2$ /$sp^3$ bonding. The buckling naturally differentiates the sublattices A and B; however for free-standing lattices, the isotropy of the system prevents the manifestation of the sublattice symmetry breaking due to buckling.

Mechanisms for breaking the sublattice symmetry have been investigated for 2D materials and includes (but are not limited to): mechanical strain (silicene nanoribbons) [10,11], chemisorption of H atoms (silicene/germanene) [12], chemisoprtion of Li atoms [13], substrate interaction (graphene) [14] and external electric fields (silicene) [15-17].

In this deliverables report , we present first-principles calculations on free-standing silicene and germanene functionalization by means of mechanical strain (uniaxial and biaxial, compressive and tensile), as well as the combination of mechanical strain and a perpendicular electric field to induce a meaningful energy bandgap for MOSFETs-type device applications. The possible mechanical strain of silicene on Ag(111) was recently discussed by Le Lay et al. [18].

## 2. Model

For our first-principles calculations we use density functional theory (DFT), as implemented in the SIESTA simulation suite [19]. The used atomic configurations are Si:(Ne)$3s^2 3p^2$ and Ge: (Ar)$3d^{10} 4s^2 4p^2$. The core electrons are modeled with norm-conserving Troullier-Martins pseudopotentials [20] and the valence electrons are modeled using double-zeta polarized basis set [21]. We employed a 128x128x1 Monkhorst-Pack *k*-grid, and an energy cut-off of 300 Ry. All calculations are performed in the generalized gradient approximation (GGA), using the PBE [22] exchange-correlation functional. The convergence criteria are set at 0.05 eV $Å^{-1}$ as residual force, yielding typically a 10 meV energy error and a residual stress of $10^{-3}$ eV $Å^{-1}$. The fully relaxed silicene unitcell has cell parameters *a*=*b*=3.87 Å and a vacuum layer of *c*=20 Å; α=β=90°, γ=120°. The fully relaxed germanene unitcell has cell parameters *a*=*b*=4.03 Å and a vacuum layer of *c*=20 Å; α=β=90°, γ=120°.

### *2.1 Mechanical Strain*

Starting from the fully relaxed unitcell, we apply in-plane uniaxial strain ε by increasing (decreasing) the unitcell. One can define two sets of basisvectors in the silicene/germanene unitcell:

$$\vec{a}_1^{zz} = a\begin{pmatrix}1\\0\end{pmatrix}, \qquad \vec{a}_2^{zz} = \frac{a}{\sqrt{10}}\begin{pmatrix}1\\3\end{pmatrix} \quad (i); \qquad \vec{a}_1^{ac} = a\begin{pmatrix}0\\1\end{pmatrix}, \qquad \vec{a}_2^{ac} = \frac{a}{2}\begin{pmatrix}\sqrt{3}\\-1\end{pmatrix} \quad (ii).$$

Vectors (*i*) couple an atom of sublattice A to atoms of the same sublattice and define the zigzag direction and vectors *(ii)* couple an atom on sublattice A to atoms of the other sublattice B and define the armchair direction. All vectors are normalized with respect to the silicene/germanene bondlength *a*. The vectors are linked by a 30 degree rotation in the case of hexagonal symmetry [23].

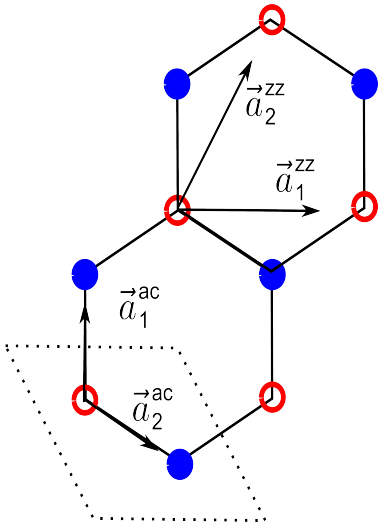


(Figure 1) The four uniaxial strain directions considered in this work. The two sublattices are indicated by the filled and open circles. The dotted line indicates the unit cell.

In-plane uniaxial strain ε in the $\vec{a}_i$ direction is defined as $\epsilon = \left( C_{\vec{a}_i}^{strained} - C_{\vec{a}_i}^{relaxed} \right) / C_{\vec{a}_i}^{relaxed}$, where ε>0 indicates tensile strain and ε<0 indicates compressive strain. In-plane biaxial strain is defined analogously, i.e. $\epsilon = \left( C_{zz,ac}^{strained} - C_{zz,ac}^{relaxed} \right) / C_{zz,ac}^{relaxed}$. For homogeneous biaxial strain, the two basisvector sets are identical. The atoms are fixed in the direction of applied strain. The magnitude of applied strain is considered up to 10%, where the deformation is elastic, cf.figure (2) [10].

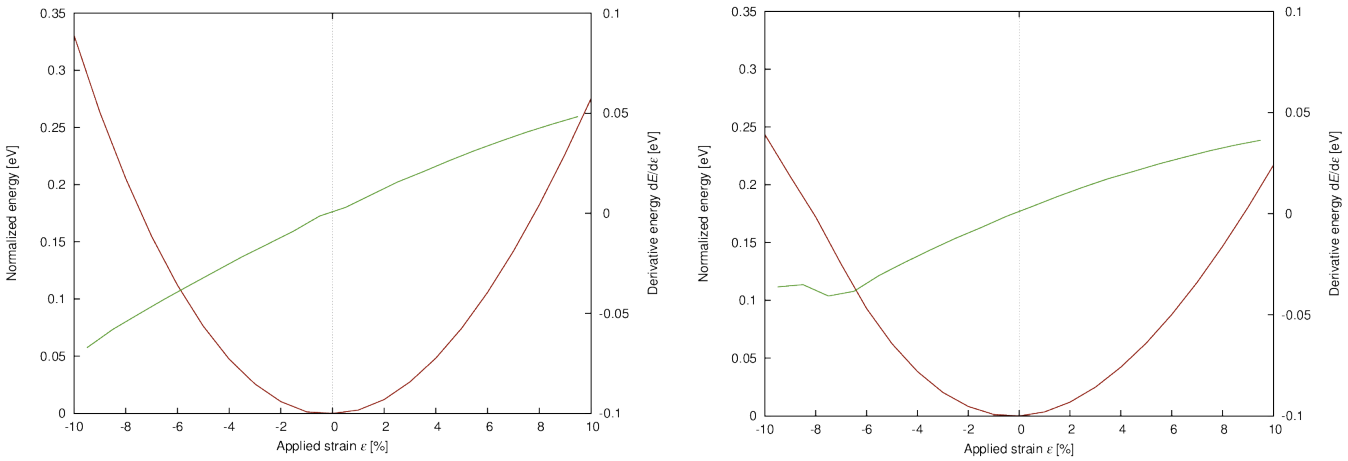


Figure (2) Free-standing silicene with zz-uniaxial strain (left), free-standing germanene with zz-uniaxial strain (right). The red curve corresponds to the total system energy with respect to the relaxed system energy (left *y*-axis). The green curve correspond to the derivative of the total energy curve (right *y*-axis). The energy is quadratic in applied strain; the deformation is elastic.

When mechanically straining the unitcell, two effects should be taken into account: valley polarization and orbital overlap. Considering this, the possible strain configurations are given in figure (3). Uniaxial strain breaks the sublattice symmetry, illustrated in figure (3, left) and introduces a bandgap, equation (2). The electronic structure also depends on the effects of the valence orbital overlap. Biaxial strain retains the sublattice symmetry; only the valence orbital overlap affects the electronic structure, see figure (3), right.

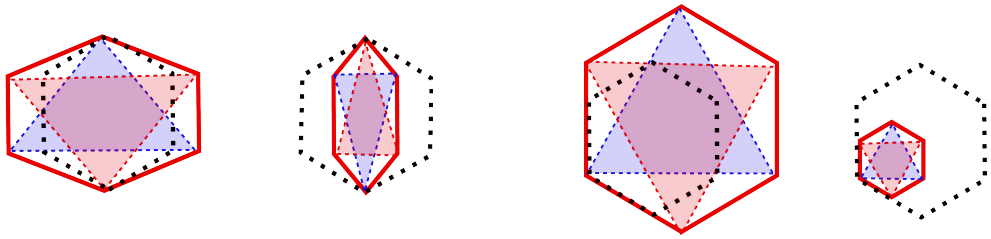

Figure (3) The original real-space hexagon is indicated with the dashed edges, the real-space strained hexagon is indicated with the solid edges and the two sublattices are indicated as filled triangles. (left) Uniaxial compressive (tensile) strain; the sublattice symmetry is broken, the valence $p_{x,y}$ orbital overlap increases (decreases). (right) Biaxial compressive (tensile) strain; the sublattice symmetry remains and the valence $p_{x,y}$ orbital overlap increases (decreases).

## 3. Results

The electronic structures presented here yield the maximal energy bandgap for the indicated strain direction(s). Larger strain magnitude results in a semimetallic electronic structure, which is undesirable from a functionalization point of view.

### *3.1 Uniaxial strain: Poisson ratio*

The buckling distance increases with applied compressive strain and decreases with applied tensile strain for both materials, as shown in figures 4. This yields a Poisson ratio $\nu_{zz}=\partial d/\partial C_{zz}=0.267\pm0.011$ for silicene and $0.120\pm0.016$ for germanene, in good agreement with previous calculations [9,10].

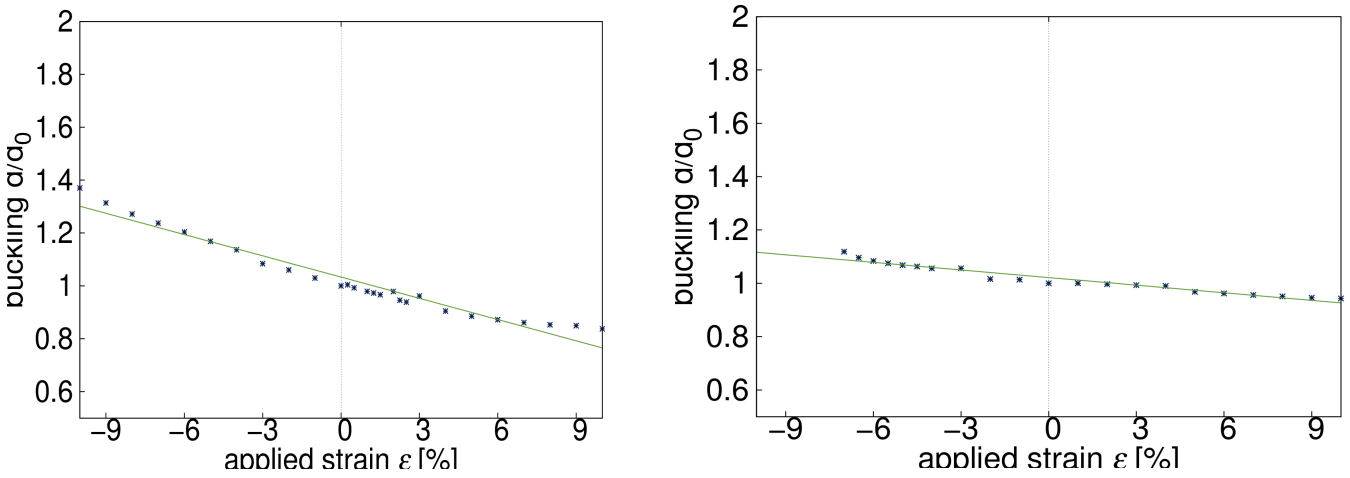


Figure (4) Relative buckling $d/d_0$ as function of uniaxial strain (zz1), with $d_0$ being the buckling distance of the unstrained monolayer. (left) Silicene. (right) Germanene.

### *3.2 Uniaxial strain: zigzag direction*

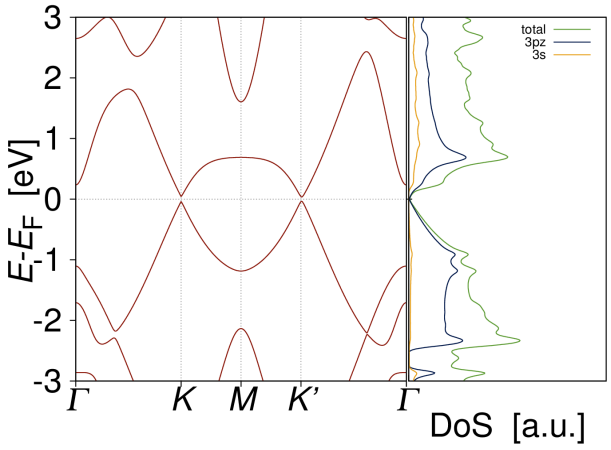


(a) Si zz1-uniaxial strain; ε=10%.

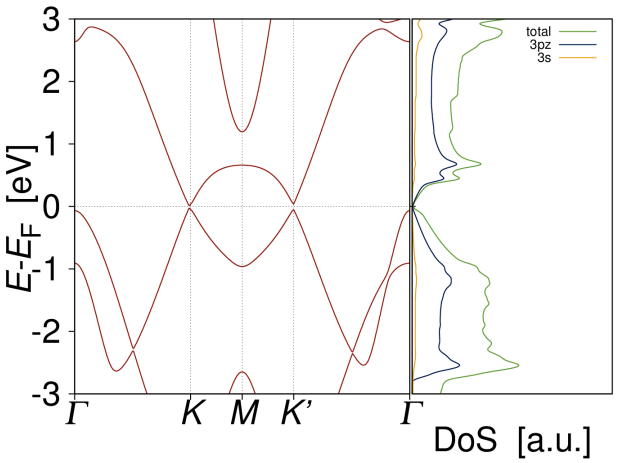


(b) Si zz1-uniaxial strain; ε=-7%.

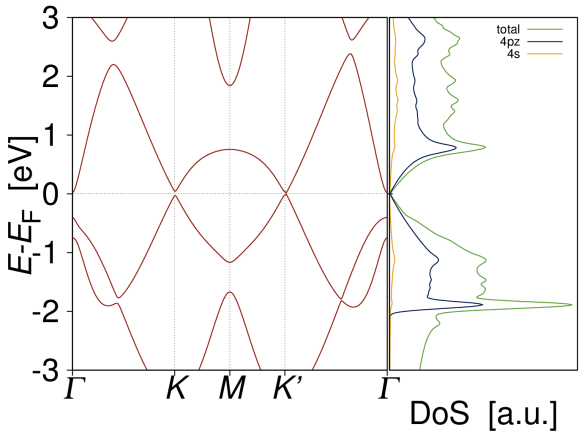


(c) Ge zz1-uniaxial strain; ε=6%.

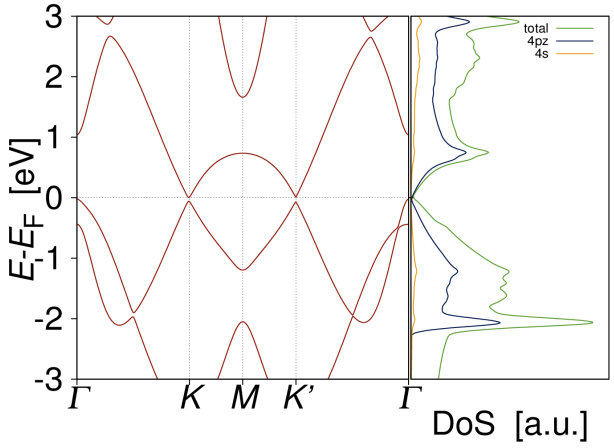


(d) Ge zz1-uniaxial strain; ε=-3%.

Figure (5) The impact of zz1 strain on the electronic structure of free-standing silicene and germanene. The left inset of the figures shows the electronic dispersion along the *ΓKMK'Γ* path in the Brillouin zone, the right inset shows the total DoS (green), valence $p_z$ orbital DOS (blue) and valence s orbital DOS (yellow).

For both materials, (1,0) direction (zz1) tensile strain induces a bandgap of 0.12 eV for silicene (ε=10%, direct), see figure (5a) and 0.06 eV for germanene (ε=6%, indirect), see figure (5c). The Dirac cones at *K* and *K'* are shifted symmetrically with respect to the Fermi energy and the density of states is zero in the gap. The former is attributed to breaking of the sublattice symmetry and the latter to the decreasing of the orbital overlap, i.e. a decrease of π bond. The bandgap energy $E_{gap}$ varies linearly with the strain magnitude, corresponding to sublattice symmetry breaking. In the case of silicene, zz1 compressive strain induces a

bandgap of 0.10 eV (ε=-7%, direct), the orbital overlap effects adding additional features, as shown in figure (5b). For germanene, we have a bandgap of 0.08 eV (ε=-3%, direct), see figure (5d). For relaxed germanene, the conduction and valence band at the *Γ* lie close to the Fermi energy (0.7 eV and 0.3 eV respectively), as opposed to silicene (2.0 eV and 1.0 eV respectively). Combining this with the fact that the the DoS at the *Γ* point is mainly due to the $p_{x,y}$ orbitals, tensile strain results in an increase of electrostatic energy and shifting the bands upwards and compressive strain shifts the bands downwards. This results in a semiconductor-semimetal transition at 6% tensile and 3% compressive strain, still well within the elastic regime, cf. Figure 2.

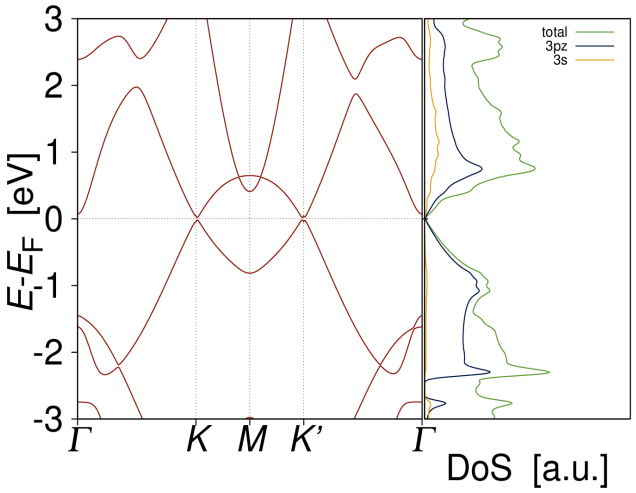


(a) Si zz2-uniaxial strain; ε=10%.

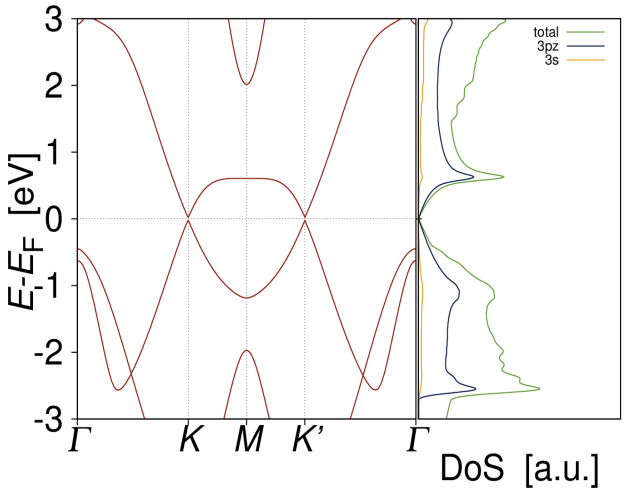


(b) Si zz2-uniaxial strain; ε=-5%.

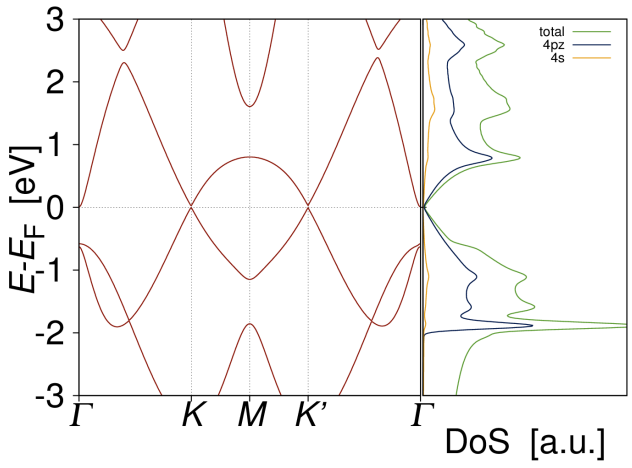


(c) Ge zz2-uniaxial strain; ε=5%.

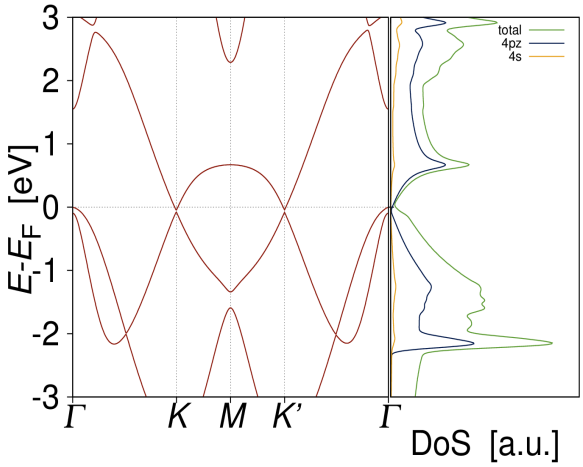


(d) Ge zz2-uniaxial strain; ε=-5%.

Figure (6) The impact of zz2 strain on the electronic structure of free-standing silicene and germanene. The left inset of the figures shows the electronic dispersion along the *ΓKMK'Γ* path in the Brillouin zone, the right inset shows the total DoS (green), valence $p_z$ orbital DoS (blue) and valence s orbital DoS (yellow).

Applying strain in the (1,3) (zz2) direction opens a band gap, figure (6a)-(6c) of 0.10 eV for silicene (10%, direct) and 0.04 eV for germanene (5%, direct). The emergence of a bandgap for this particular strain direction is understood as enlarging/shrinking a particular triangular sublattice (A) with respect to the other sublattice (B). It is understood that the vectors $\vec{a}_{1^{zz}}$ and $\vec{a}_{2^{zz}}$ are identical with respect to the hexagonal lattice and triangular sublattice symmetries and applying strain in any of these directions should yield an identical electronic structures. However, we have distinguished between these cases since the triagonal symmetry is not retained for the zigzag basisvectors, thus being not retained for the silicene or germanene unitcell, nor for a (*n* x *m*) supercell. So, we consider both vectors as distinct fundamental building blocks of any 2D Si (Ge) superstructure [16], for example the (3x3) silicene superstructure on Ag(111), where the bond lengths are tensile strained up to 3%, but where the supercell symmetry is not hexagonal.

### *3.3 Uniaxial strain: armchair direction*

Applying strain in the armchair (0,1) (ac1) direction opens a bandgap as well, figure (7), but it is of a slightly different nature than the behaviour of zigzag direction straining. Applying tensile strain in the zigzag (√3,-1) (ac2) direction opens a bandgap only for silicene (0.10 eV, ε=10%, direct), see figure (8a), but not for germanene (fiigure 8b). Compressive strain in the ac2-direction does not result in a bandgap, figures (8b) ans (8d). The emergence of a bandgap for this particular tensile strain direction in silicene is understood as enlarging/shrinking a particular triangular sublattice (A) with respect to the other sublattice (B).

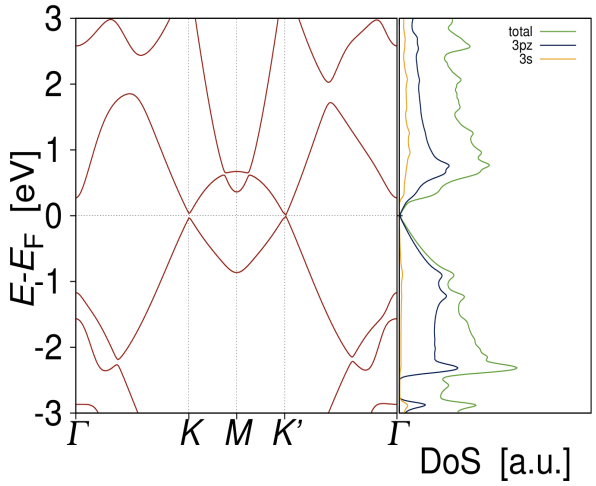


(a) Si ac1-uniaxial strain; ε=10%.

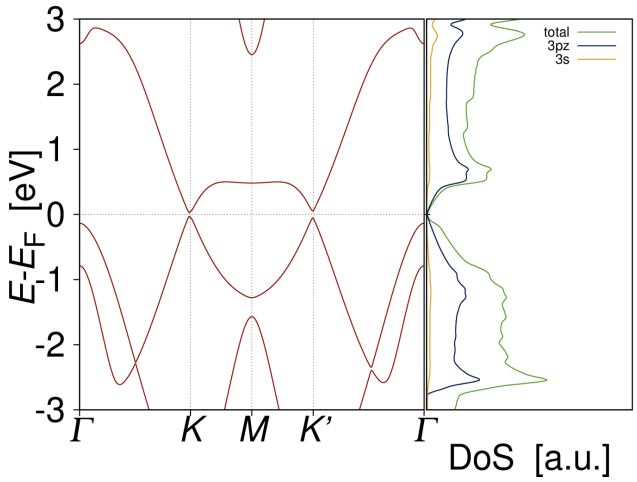


(b) Si ac1-uniaxial strain; ε=-7%.

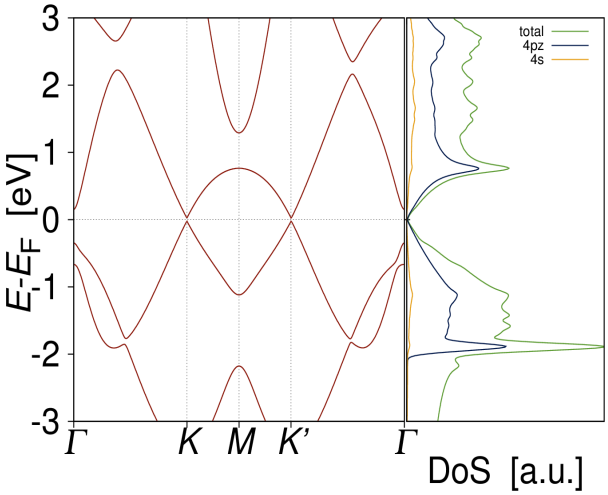


(c) Ge ac1-uniaxial strain; ε=5%.

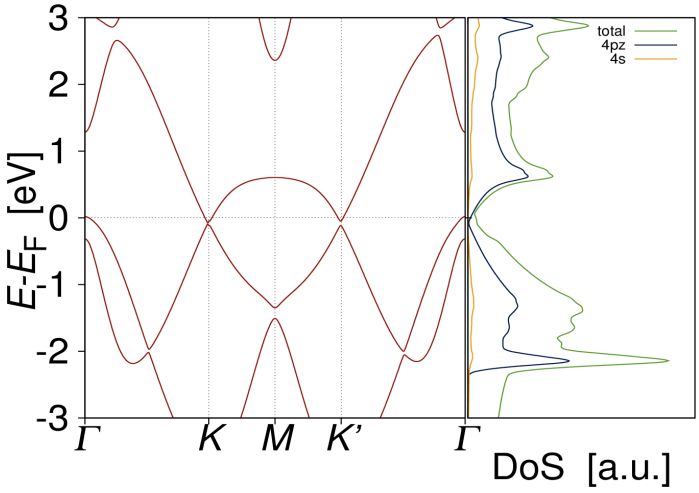


(d) Ge ac1-uniaxial strain; ε=-5%.

Figure (7) The impact of ac1 strain on the electronic structure of free-standing silicene and germanene. The left inset of the figures shows the electronic dispersion along the *ΓKMK'Γ* path in the Brillouin zone, the right inset shows the total DoS (green), valence $p_z$ orbital DoS (blue) and valence s orbital DoS (yellow).

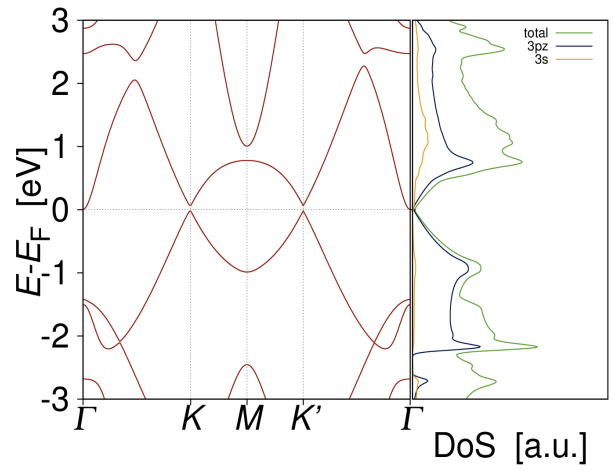


(a) Si ac2-uniaxial strain; ε=10%.

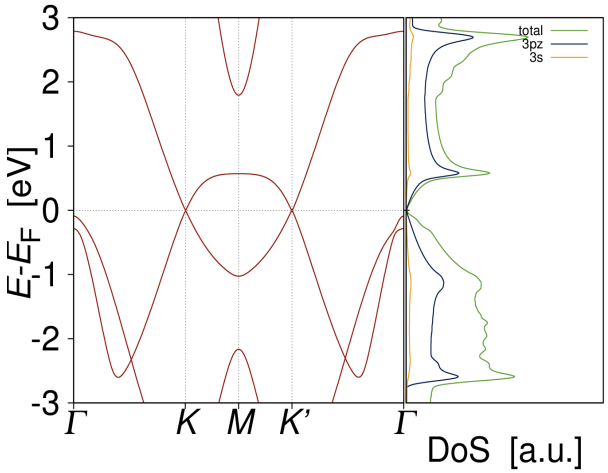


(b) Si ac2-uniaxial strain; ε=-7%.

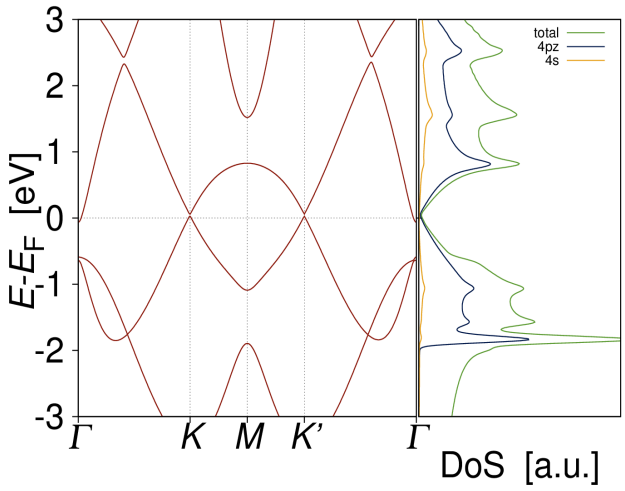


(c) Ge ac2-uniaxial strain; ε=5%.

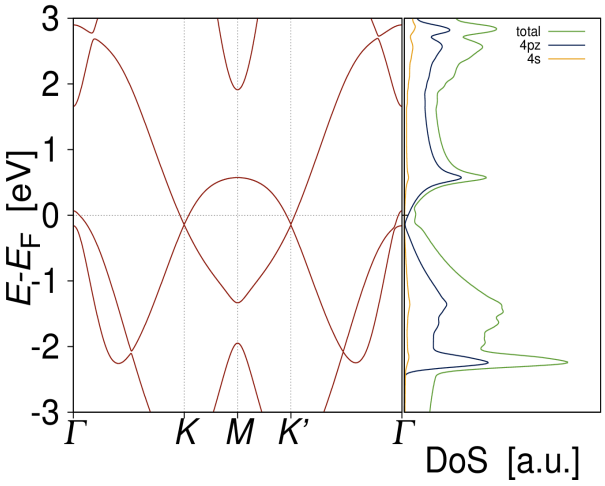


(d) Ge ac2-uniaxial strain; ε=-5%.

Figure (8) The impact of ac2 strain on the electronic structure of free-standing silicene and germanene. The left inset of the figures shows the electronic dispersion along the *ΓKMK'Γ* path in the Brillouin zone, the right inset shows the total DoS (green), valence $p_z$ orbital DoS (blue) and valence s orbital DoS (yellow).

### *3.4 Biaxial strain*

Homogeneous biaxial strain (h-b) retains the sublattice symmetries, figure (2), and thus is not expected to introduce a bandgap, which is consistent with our calculations, presented in figure (9). The *K* and *K′* points are crossing the Fermi level, giving a metallic electronic structure [24]. For hb strain, both tensile (9a)-(9c) and compressive (9b)-(9d), the electronic properties tend to those of a semimetal; with a critical strain of ±6√2% for silicene and ±3√2% for germanene.

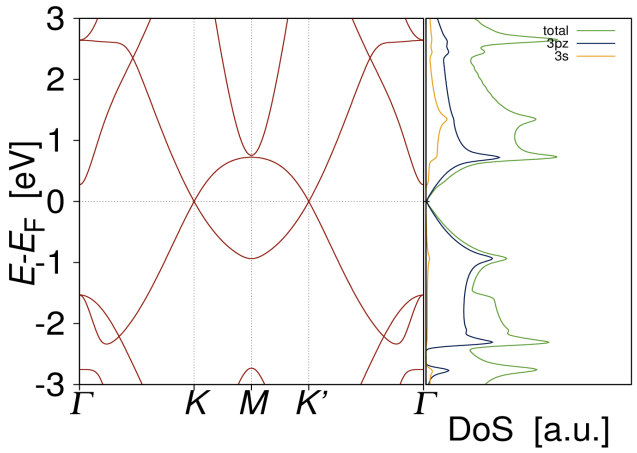


(a) Si h-b strain; ε=6√2%.

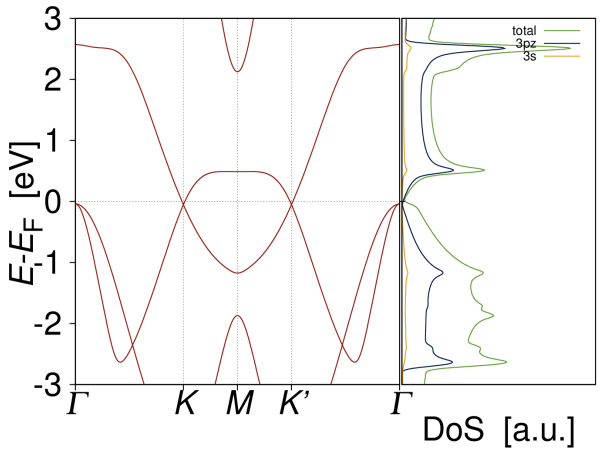


(a) Si h-b strain; ε=-6√2%.

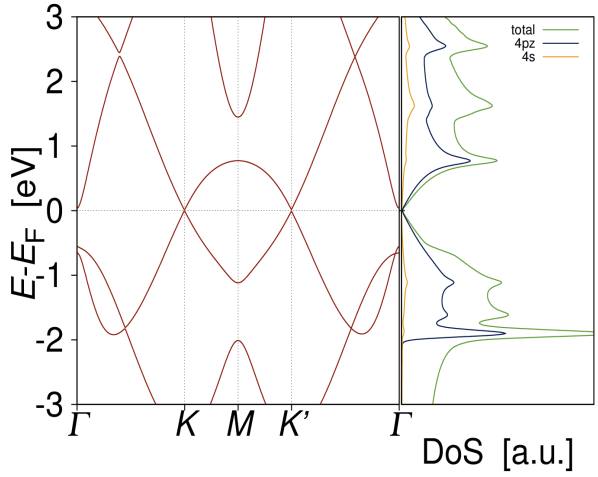


(c) Ge h-bl strain; ε=3√2%.

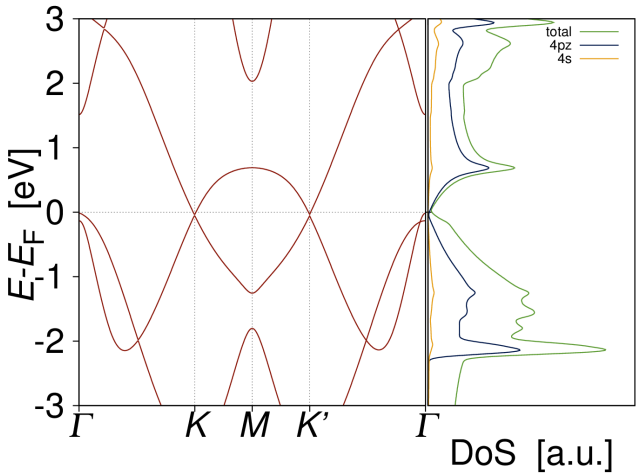


(d) Ge h-b strain; ε=-3√2%.

Figure (9) The impact of h-b strain on the electronic structure of free-standing silicene and germanene. The left inset of the figures shows the electronic dispersion along the *ΓKMK′Γ* path in the Brillouin zone, the right inset shows the total DoS (green), valence $p_z$ orbital DoS (blue) and valence s orbital DoS (yellow).

Very interestingly, non-homogeneous biaxial strain (non-hb) yields the largest (direct) bandgap for both silicene and germanene. The semiconductor-semimetal transition occurs at the *Γ* point when the conduction (valence) band crosses the Fermi level for tensile (compressive) strain. Keeping the ratio $\varepsilon_x/\varepsilon_y$ which is indicative of a certain strain direction, we note a bandgap of 0.18 eV for silicene (10a) and 0.06 eV for germanene (10b). Note that in the case of germanene, non-hb strain allows for larger magnitudes than $3\sqrt{2}\%$.

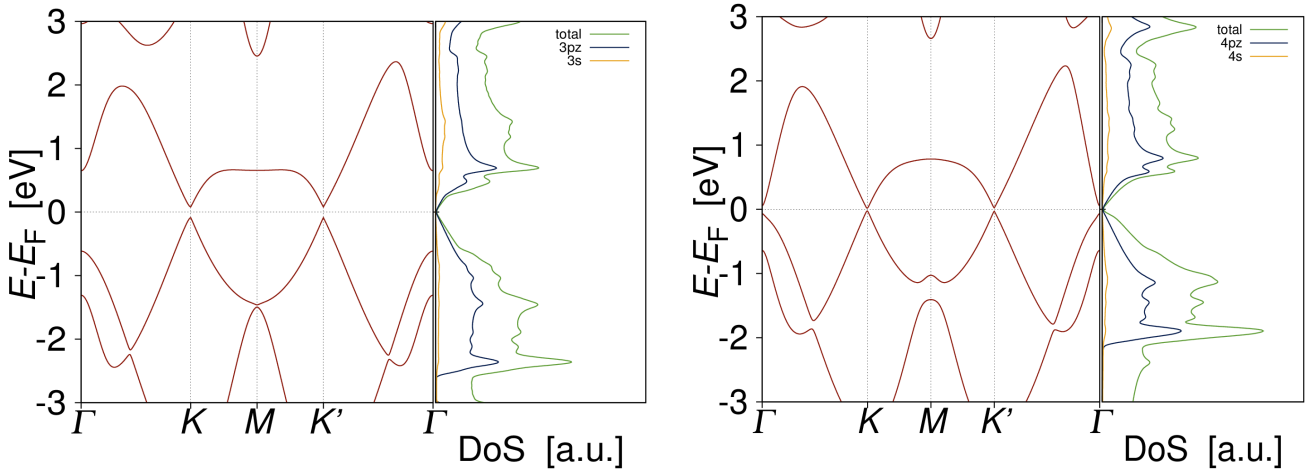


(10a) Si non-hb strain, zz2 direction; $\varepsilon_x$=9.5%, $\varepsilon_y$=-5.5% (10b) Ge non-hb strain, zz2 direction; $\varepsilon_x$=9.5%, $\varepsilon_y$=-5.5%

### *3.5 Applied electric field*

Motivated by recent findings on topological phases in silicene induced by applying an electric field to the material [15], we consider the effect of an electric field $E_z$ applied perpendicular to the silicene/germanene layer, up to 1 V $Å^{-1}$. By breaking the isotropy of the system, combined with the intrinsic buckling of the Si and Ge monolayers, the inversion symmetry is broken. Now one can distinguish between a 'top' and a 'bottom' Si atom via charge transfer. Charge transfer between the 'bottom' Si atom and 'top' Si atom increases linearly with applied electric field (see Ref. [25]). The sublattice symmetry is broken, contrary to (monolayer) graphene [26], where spin-orbit coupling is needed to break the inversion symmetry.

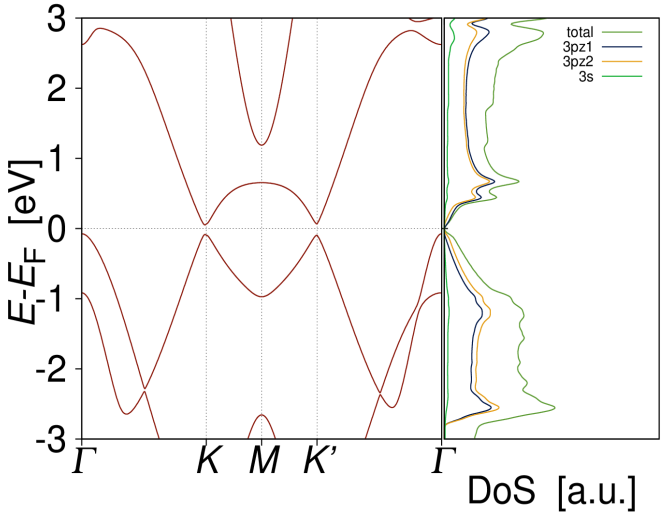


(a) Electronic dispersion and DoS for ε=-7% zz strained silicene, $E_z$=1 V Å$^{-1}$.

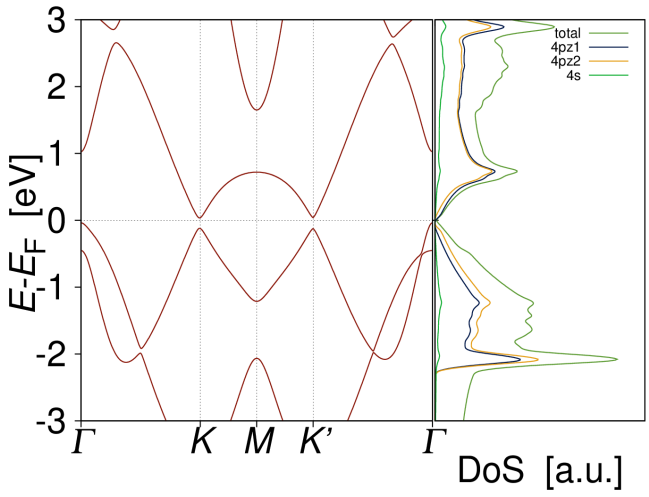


(b) Electronic dispersion and DoS for ε=-3% zz strained germanene, $E_z$=1 V Å$^{-1}$.

Figure (11) Combining compressive strain and a perpendicular electric field yield a compounded bandgap magnitude. The left inset of the figures shows the electronic dispersion along the *ΓKMK'Γ* path in the Brillouin zone, the right inset shows the total DoS (green), valence $p_z$ orbital DoS (blue for the 'top' atom, yellow for the 'bottom' atom) and valence s orbital DoS (green).

The bandgap energy increases linearly with the applied electric field, up to 0.14 eV for silicene (0.15 eV for germanene) and a Mulliken charge transfer from the 'top' atom to the 'bottom' atom of 0.09*e* (0.11*e* for germanene) is calculated – which reflects the polarization of the $p_z$ orbitals, which differ for the 'top' and the 'bottom' atom near the Fermi energy. Combining uniaxial strain and electric field leads to a compounded bandgap; electrostatic shifting of the energy of the Dirac cones (linear in applied field $E_z$ and linear in buckling distance *d*) and breaking of the sublattice symmetry (linear in the buckling distance *d*). This results a maximal bandgap of 0.21 eV for silicene (direct), figure 11 (a), and 0.15 eV for germanene (indirect), figure 11 (b).

Choosing the compressive critical strain magnitude yield the largest compounded bandgap since the perpendicular field affect the valence $p_z$ orbitals and not the valence $p_{x,y}$ orbitals. The Fermi level crossing of the valence band at the *Γ* point happens at the same critical strain magnitude. Hence the semiconductor-semimetal transition point does not change.

Non-homogeneous biaxial strain results in the largest computed bandgap, but also to a smaller buckling distance, and, consequentely a smaller compounded bandgap effect.

## 4. Conclusions

In this report, we have investigated the functionalization of silicene and germanene by means of mechanical strain and perpendicular electric fields. A band gap is introduced at the *K* and *K'* high symmetry points by breaking the sublattice symmetry. This is reflected by the application of uniaxial strain to the system, which yield a semiconducting electronic structure, as opposed to biaxial strain which yield a generic semimetallic electronic structure. The two basissets used to define the strain directions are equivalent if both the hexagonal and triangular symmetry of the honeycomb lattice is retained in the unitcell; However, when the system is strained in a specific direction (uniaxially), the hexagonal symmetry is not retained, and the electronic structure obtained with respect to the different basisvectors differs in the magnitude of the energy bandgap, as well as in the dispersion near the *M* point.

In general, we conclude that silicene is more suited to functionalization by mechanical strain as opposed to germanene. First, uniaxial straining of the unitcell induces a maximal gap of 0.12 eV for silicene for 10% tensile strain in the zigzag direction (0.04 eV for germanene, 6% zigzag tensile). The bandgap opening grows linear with the strain magnitude, which indicates that the gap opening can be attributed to sublattice symmetry breaking. Biaxial compressive strain does not break sublattice symmetry and the electronic structure is determined by the overlap of the valence $p_{x,y}$ orbitals, yielding a semimetallic-like behaviour, due to the crossing of the Fermi level at the $\Gamma$ point. Very interestingly, when the system is tensely strained in one direction and compressively strained in the another direction, we allow for a redistribution of $p_{x,y}$ population and breaking of the sublattice symmetry in the same (linear) fashion. This procedure yields a bandgap of 0.18 eV for silicene ($\varepsilon_x$=9.5%, $\varepsilon_y$=-5.5%, zz2 direction) and 0.06 eV for germanene ( $\varepsilon_x$=9.5%, $\varepsilon_y$=-5.5%, zz2 direction).

Applieding an electric field $E_z$ induces a gap of ~0.10 eV by breaking the system isotropy and manifests the buckled nature of silicene and germanene. Combining strain and electric field yield maximal bandgaps of 0.21 eV for silicene and 0.15 eV for germanene and offers perspectives for application of silicene and germanene in devices.

Applying an electric field to a silicene/germanene superstructure on a (insulating) substrate is the subject of current investigations.

## References


[1] A.H. Castro Neto, F. Guinea, N.M.R. Peres, K.S. Novoselov, A.K. Geim, Rev. Mod. Phys. **81**, 109, (2009).

[2] P. Vogt, P. De Padova, C. Quaresima, J. Avila, E. Frantzeskakis, M.C. Asensio, A. Resta, B. Ealet, G. Le Lay, Phys. Rev. Lett. **108**, 155501, (2012).

[3] D. Chiappe, C. Grazianetti, G. Tallarida, M. Fanciulli, A. Molle, Adv. Mat. **24**, 5088, (2012).

[4] A. Fleurence, R. Friedlein, T. Ozaki, H. Kawai, Y. Wang, Y. Yamada-Takamura, Phys. Rev. Lett. **108**, 245501, (2012).

[5] M. Houssa, G. Pourtois, V. V. Afanas'ev, A. Stesmans, Appl. Phys. Lett. **97**, 112106, (2010).

[6] M. Houssa, G. Pourtois, V. V. Afanas'ev, A. Stesmans, Appl. Phys. Lett. **96**, 082111, (2010).

[7] F. Schwierz, Nature Nanotech. **5**, 487, (2010).

[8] M.Z. Hasan & C.L. Kane, Rev. Mod. Phys. **82**, 3045, (2010).

[9] S. Cahangirov, M. Topsakal, E. Ataturk, H. Sahin, S. Ciraci, Phys. Rev. Lett. **102**, 236804, (2009).

[10] R. Qin, C-H. Wang, W. Zhu, Y. Wang. AIP Advances **2**, 022159, (2012).

[11] M. Topsakal, S. Ciraci, Phys. Rev. B **81**, 024107, (2010).

[12] M. Houssa, E. Scalise, K. Sankaran, G. Pourtois, V. V. Afanasev, A. Stesmans, Appl. Phys. Lett. **98**, 223107, (2011).

[13] T.H. Osborn & A.A. Farajian, J. Phys. Chem. C **116**, 22916, (2012).

[14] G. Giovannetti, P.A. Khomyakov, G. Brocks, P.J. Kelly, J. van den Brink, Phys. Rev. B **76,** 073103, (2007).

[15] M. Ezawa, Phys. Rev. Lett **109**, 055502, (2012).

[16] M. Ezawa, cond-mat/arXiv:1209.2580 29, (2012).

[17] M. Houssa, B. van den Broek, E. Scalise, G. Pourtois, V.V. Afanas'ev, A. Stesmans, *submitted.*

[18] G. Le Lay, P. De Padova, A. Resta, T. Bruhn and P. Vogt, J Phys D **45**, 392001 (2012).

[19] J.M. Soler, E. Artacho, J.D. Gale, A. Garcia J. Junquera, P. Ordejon, D. Sanchez-Portal, J. Phys. C: Cond. Matter **14**, 2745, (2002).

[20] N. Troullier & J.L. Martins, Phys. Rev. B **43**, 1993, (1991).

[21] F. Jensen, Introduction to Computational Chemistry, Wiley, (2007).

[22] J. Perdew, K. Burke, M. Ernzerhof, Phys. Rev. Lett. 77, 3865, (1996).

[23] M. Bishop, Group Theory and Chemistry, Dover, (1973).

[24] S.-H. Lee, S. Kim, K. Kim, Phys. Rev. B **86**, 155436, (2012).

[25] N.D. Drummond, V. Z´lyomi, V.I. Fal'ko, Phys. Rev. B **85**, 075423, (2012).

[26] H. Min, B. Sahu, S.K. Banerjee, A.H. MacDonald, Phys. Rev. B **75**, 155115, (2007).